in [7]. Sequence data for type III collagen come from bovine skin collagen and was kindly given to us by Dr. J. Chapman and Dr. M. Humphries. Although these sequence data do not come from the same species used in this work this is not a problem, as a substantial measure of homology between species exists.

Five liver and six skin images from two different species are analyzed using the proposed approach. For each image we derive a single average D-period, so that each set is described by a small number of average D-periods. The D-periods of each set are being aligned to each other and to model I as reference. We then average them and get an overall average D-period for each set (total set). Next, we employ the proposed pattern analysis procedure to derive type I tendencies for each average D-period, i.e., for each set.

Table I summarizes our results. The field named "number of periods" records the number of periods that the D-period extraction algorithm samples from the current image. The subsequent "type I proportion" field records the proportion a of model I at the mixture model that was found to correlate at the highest degree with the corresponding average D-period, and the field "correlation coefficient" encodes the degree of correlation between this mixture model and the average image D-period. The row labeled "Total Set" presents the results corresponding to the overall D-period of the entire set. A first comparison indicates that the relative amount of type I periods is larger in liver than in skin fibrils. Indeed, the relative type I tendencies for liver and skin sets are respectively 94% and 91%. Our results are in good agreement with those derived from biochemical methods [3] confirming that liver contains an assortment of collagen types, usually with type I predominating, though this is not always the case. Skin has a different overall profile from other tissues. Two collagen types, I and III, are the main constituents accompanied by other minor types.

The significance of the derived linear proportion coefficients is tested via statistical hypothesis tests. We validate the ability of a single average period (for the total set) to represent the sample population, in respect to proportion of and correlation with the mixture model. In order to assess results concerning the agreement of a sample mean $\bar{x}$ with the overall D-period measure μ derived (tested mean), we set up a statistical hypothesis test for type I proportion of the form

$$\mathrm{H}_{0:}\bar{x} = \mu, \text{ versus } \mathrm{H}_{1:}\bar{x} \neq \mu.$$

For sample size and standard deviation m and s, respectively, the test statistic $t_1 = |(\bar{x} - \mu)/(s/\sqrt{m})|$ is compared against the one-sided threshold for the significance level a, which is specified as the upper $a/2$ percentile of the t-distribution with $m-1$ degrees of freedom. The test statistics with the corresponding thresholds at 10% significance are also in the Table I. Overall, it is derived that the total set measures are in good agreement with the sample means, i.e., the test statistic cannot reject the null hypotheses.

V. Conclusion

In this work we explore the potential for automatic analysis of microscopic images from periodic-fibrillar structures. We introduce a pattern matching approach for the analysis and comparison of average D-periods with sequence generated histograms. This algorithm aims in deriving the relative content of type I collagen, but it can be easily modified to deal with other types of fibrillar proteins (theoretical models).

We plan to extend this approach to study interactions among various types of collagen testing normal and pathological tissue of several types and ages.

References

[1] B. Eyden and M. Tzaphlidou, "Structural variations of collagen in normal and pathological tissues: Role of electron microscopy," *Micron.*, vol. 32, pp. 287–300, 2001.

[2] J. A. Chapman, M. Tzaphlidou, K. M. Meek, and K. E. Kadler, "The collagen fibril—A model system for studying the staining and fixation of a protein," *Electron Microsc. Rev.*, vol. 3, pp. 143–182, 1990.

[3] J. Weiss, "Collagens and collagenolytic enzymes," in *Connective Tissue Matrix*, D. W. L. Hukins, Ed. Weinheim, Germany: Verlag Chemie, 1984, pp. 17–53.

[4] C. M. Black, V. C. Duance, T. J. Sims, and N. D. Light, "An investigation of the biochemical and histological changes in the collagen of the kidney in systemic sclerosis," *Collagen Related Res.*, vol. 3, pp. 231–243, 1983.

[5] E. J. Waterhouse, P. J. Quesenberry, and G. Ballian, "Collagen synthesis by murine bone marrow cell culture," *J. Cell. Physiol.*, vol. 127, pp. 397–402, 1986.

[6] J. A. Chapman, D. F. Holmes, K. M. Meek, and C. J. Rattew, "Electron-optical studies of collagen fibril assembly," in *Structural Aspects of Recognition and Assembly in Biological Macromolecules*, M. Balaban, J. L. Sussman, W. Traub, and A. Yonath, Eds. Rehovot, Philadelphia, Israel: International Science Services, 1981, pp. 387–401.

[7] J. B. Weiss and M. I. V. Jayson, *Collagen in Health and Disease*. Edinburgh, U.K.: Churchill Livingstone, 1982.

A High-Throughput 3-D Composite Dielectrophoretic Separator

Henry O. Fatoyinbo, David Kamchis, Reginald Whattingham, Stephen L. Ogin, and Michael P. Hughes*

***Abstract*—Dielectrophoresis has great potential to offer a range of diverse fields from bioprocessing to clinical medicine, but is hampered by low throughput rates to the micrometer scale of the electrodes required to generate highly nonuniform fields. Here we describe a novel approach to electrode construction, using a drilled laminated structure to form channels bearing electrodes 30 μm across and 150 μm apart. Since these electrodes appear along all sides of the drilled bore, the trapping efficiency is improved over conventional devices. We have developed and demonstrated a separator capable of sorting a 50:50 mixture of viable and nonviable yeast cells into an 86:14 mixture at 25 mLhr^{-1}.**

***Index Terms*—Dielectrophoresis, cell separation, microengineering.**

I. Introduction

There is a trend in biosensor development toward applying technological advances in the field of microengineering to construct "labs on a chip" (also known as micrometer-scale, total analytical systems or μTAS). These devices usually consist of integrated fluid handling, sorting, and identification components on a single glass or plastic slide, with dimensions somewhere between those of a postage

Manuscript received February 16, 2004; revised October 19, 2004. *Asterisk indicates corresponding author.*

H. O. Fatoyinbo, D. Kamchis, R. Whattingham, and S. L. Ogin are with the School of Engineering, University of Surrey, Surrey GU2 7XH, U.K.

*M. P. Hughes is with the School of Engineering, University of Surrey, Surrey GU2 7XH, U.K. (e-mail: m.hughes@surrey.ac.uk).

Digital Object Identifier 10.1109/TBME.2005.847553

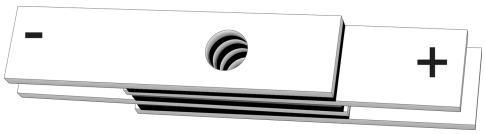

Fig. 1. A schematic showing the construction of a single bore of the device. Alternating conducting planes are excited by opposing phases from a signal generator. A typical device consists of 20 conducting layers, with hundreds of bores per separator.

stamp and those of a credit card. The advantage of such devices is that they allow the analysis of small samples rapidly, allow use of miniaturised sensing systems, and can be constructed so that the integrated fluid/sensing element (the "lab on a chip" itself) is disposable (with benefit for maintaining sterile conditions and avoiding contamination). When electrodes on the micro-scale are used, a number of techniques become available for use. AC electrokinetic phenomena such as dielectrophoresis (DEP) have been used for many years for the manipulation, separation, and analysis of cellular-scale particles. DEP is the phenomenon of attraction to, or repulsion from, regions of high electric field strength [1], [2]. Particles experiencing such forces can be made to exhibit a variety of motions including attraction, repulsion, and rotation by changing the nature of the dynamic field. The orientation and magnitude of the force or torque is related to the relative polarisabilities of the particle and suspending medium. Study of this behavior allows the determination of biophysical properties of the particles, with potential for clinical applications (e.g., [3]–[5]); unlike flow cytometry, DEP does not require fluorescent staining, as particles are differentiated by the act of attraction to, or repulsion from, the force-generating electrodes.

By exploiting the fact that different particles may experience forces in different directions when all other factors are the same, researchers have been able to use DEP to separate mixtures of cells on electrode arrays, including viable and nonviable cells, cancers, blood, and micro-organisms (as reviewed in [6]). However, these separation processes have been slow to migrate from laboratory to market because the planar nature of the flow cell needed in order to microfabricate electrodes greatly limits the throughput rate of the sample in the device. Whilst early electrodes for the DEP manipulation of cells were fabricated on the millimeter scale and employed high voltages to generate sufficient DEP forces, DEP manipulation since the late 1980s has employed pseudo-2-D electrode devices, wherein thin films (typically 100 nm) are etched away using photolithographic processes. This allows the fabrication of the micrometer-scale electrode devices required for DEP manipulation of cells at much lower voltages, but has the drawback that the working volume of cell solution that can be analyzed is very small, restricting solution throughput to a maximum of perhaps hundreds of μl/h.

In this paper we describe, for the first time, a composite three-dimensional (3-D) electrode array structure capable of increasing this throughput by over one order of magnitude; the device is capable of fabrication with micrometer-scale electrodes without requirement for access to photolithographic processing equipment or clean room facilities. The device consists of a laminate structure using conducting film 30 μm thick and insulating film 150 μm thick, with holes drilled through the laminate. The alternate conducting layers are energised with opposing phases, so that the electric field morphology along the wall of the hole is very similar to 2-D interdigitated electrode structures. However, the new device offers greater effective trapping volume and the benefits of massive parallelization (allowing much higher throughput than conventional devices) and ease of low-cost fabrication.

II. Construction

Whereas previous DEP studies have used electric fields generated by planar [effectively two-dimensional (2-D)] electrodes etched from gold films deposited across the surface of a microscope slide, the method presented here uses a conductor/composite laminate arrangement to manufacture electrodes with similar dimensions, but which can be structured along the surface of a hollow cylinder. A schematic of the device is shown in Fig. 1. The laminate consists of alternating layers of insulating and conducting material, and the conducting layers project out of the laminate on opposing sides of the device, so that the signal inputs can be connected to these projecting ends. Channels are formed through the laminate by drilling, so that each hole is equivalent to a "rolled-up" 2-D electrode array. This arrangement encloses a much larger volume than planar electrodes on a similar scale. A large number of holes can be drilled through the laminate to increase the throughput of the device.

Construction details were as follows. Aluminum foil and epoxy resin film (ACG LTA45-1; Advanced Composites Group, U.K.) were used to form the conducting and insulating layers, respectively, which were cut to size using templates of 100×100 mm and 30×100 mm, respectively. A sharp knife was adequate to cut the layers. The layers were carefully stacked by placing the epoxy layers between the aluminum layers, with alternating aluminum layers protruding from the sides. The completed structure, consisting of 20 aluminum layers and 19 epoxy layers. was placed between release film (inner) and glass plates (outer). A weight of 0.94 kg was placed on the upper glass plate to decrease the overall thickness of the structure from 6 mm to 2 mm (± 0.5 mm). The laminate was then placed in an oven and cured at 55 °C (calibrated by thermocouple) overnight for 16 h. A jig consisting of metal rods that spanned the length of the lower glass plate was constructed on the lower glass plate to ensure that the structure remained stable whilst curing. After 16 h of curing, the structure was cut into three strips with a fine tooth saw.

Following construction, a multimeter was used to determine if any electrode layers were touching by measuring the resistance between adjacent layers. Where adjacent layers were found to be conducting, which may have developed when cutting the cured structure into strips, the strips were polished down with graded sanding paper until the structures were found to be fully insulated. Holes were drilled using a computer-numerically controlled machine. Two types of separator geometry were drilled; the first with 72 $\times$ 1000 μm-diameter holes, and the second with 288×500 μm -diameter holes, written across a circular area with a radius of approximately 10 mm. The insulation test was repeated after drilling to ensure there was still no conduction path. Fig. 2 shows a cross section of a cured structure examined using an optical microscope (Zeiss Photomicroscope II, Germany). It can be seen that the thickness of the epoxy layer (black) was not constant, but varied between 130–150 μm. The aluminum foil thickness measured before curing was found to be 30 μm.

III. Simulation

It is possible to make a crude approximation of the maximum useful flow velocity through the bore by considering that the flow through the bore is equal across the cross section of the bore (though in reality, the flow profile is parabolic). We can determine the optimal flow rate through the separator by considering the maximum distance a particle can travel so as to reach the edge of the bore before the flow pushes it clear of the device, and thereby determine the effective volume from which the separator can pull particles. The DEP forces were evaluated from finite element simulations by summing the forces along the path from bore axis to bore edge using the Maxwell 3-D (Ansoft Inc, Pittsburgh, PA) field simulation suite. An example of the electric field

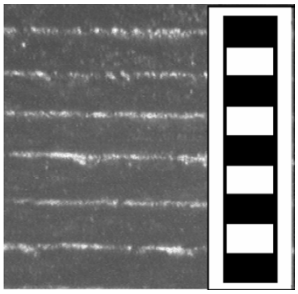

Fig. 2. A micrograph showing a cross section of a completed device, with metal electrodes (bright) sandwiched between insulating material (dark). The scale bar indicates 100 μm between divisions.

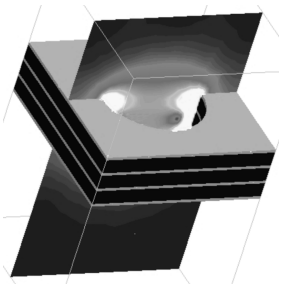

Fig. 3. An electric field simulation showing the field strength distribution in a simple 4-conductor bore, with field strengths shown from 0 Vm^{-1} (black) to 3×10^4 Vm^{-1} (white). Note that although the system is axisymmetric, there is a field gradient visible across the entrance of the hole that may attract particles toward the outer bore edge; there is also a toroidal field null approximately halfway between the axis and the edge.

through a simplified bore containing four electrodes is shown in Fig. 3. The optimal bulk flow rate through the chambers, allowing enough time for particles to collect, can be found using the longest time it takes a particle to reach the wall for the 1000-μm and 500-μm bores. Since the radial force in an axisymmmetric system is zero, it is possible to define a "useable volume," based on the time taken for a particle to travel from the edge of that volume to be trapped at the electrodes for given conditions of applied potential and the dielectric properties of the system. From the finite element simulations, a lower threshold for the electric field equating to a force of 10 pN was found, and under these conditions, the average time it takes for a particle to travel the distance from the inner edge of the useable volume to the bore wall was found to be 10.45 s for the 500-μm bore chamber and 285 s for the 1000-μm bore chamber. The optimal volumetric flow rate through each bore in order to achieve this was calculated to be 22 μl/h^{-1} and 87 μl hr^{-1} for the 1000 μm and 500 μm bores, respectively. The total volumetric flow required to pass through the cell separators is found simply by multiplying the volumetric flow rate by the respective number of bores. The total volumetric flow rate for bore diameters of 1000 μm (71 holes) and 500 μm (288 holes) are 1.82 μl/h $^{-1}$ and 25 μl/h^{-1}, respectively. Since only those cells within the volume between the bore wall and the limit of dielectrophoretic force will be separated in this time, it is possible to determine how many cells of the total are likely to be collected by calculating the ratio of the total bore volume and the volume in which trapping is effective. Results suggest that 75% of the 500-μm-diameter chamber is effective, whilst only 25% of the 1000-μm-diameter chamber is effective. Assuming all cells within the effective volume are separated, then an initial 50:50 mix of two cell populations would contain a ratio of about 87:13 after separation in devices with 500 μm bores, and 63:37 separation in devices with 1000 μm bores after a single pass. This figure is not immutable, but depends on the flow rate; where flow is slower, the particles have more time to move from the chamber and so more particles can be separated.

IV. Experimental Results

In order to test the device, yeast cells (*S.cervisiae)*, strain CG-1945^{e}, were cultured in YPD media (Sigma Aldrich). An aliquot of live cells were rendered nonviable by heat-treatment in a water bath at 90 °C for 30 min. Viable and nonviable cells were resuspended in 280 mM mannitol. Cells were counted using a hemacytometer, and mixed in a 50:50 ratio (total cell concentration 1.95×10^7 cells ml^{-1}, final volume 10 ml). Methylene blue was used to distinguish between live and dead yeast cells, as described by Lee *et al.* [7]. A 20-MHz function generator (Thurlby-Thandar Ti1000, Huntingdon, UK) was used to supply a sinusoidal 10-MHz, 10-V ac signal to the separator. A syringe pump (Model A-99, Razel Scientific Instrument) was used to pump cell solution through the separator using the flow rates calculated above. The tubing and the separator were washed with distilled water at 100 mLhr^{-1} before and after each experiment to clear cells and other debris from previous experiments. For the 500-μm bore chambers, the average percentage of viable cells collected was 86%, with 14% of cells in the eluted sample being nonviable. For separators with a bore size of 1000-μm diameter, a mean percentage of 73% of cells collected were viable cells, and 27% were nonviable. The device with smaller bore hole diameters did show a higher mean percentage of viable cells collected than for the larger bore diameters, despite being driven at a significantly higher flow rate. The number of cells of both populations agrees well with the predictions from the electric field simulations, particularly for the 500-μm bores where there was a 1% difference between predicted and measured ratios of separated particles. Although the overall agreement between theory and experiment is reasonable, there are a number of possible sources of error. Not only have approximations been made in the simulations, but the longer the separator took to flush the cells through the separator, the longer is the period of time during which viable cells can reproduce and change the recorded result.

V. Conclusion

In conclusion, this novel 3-D dielectrophoretic separation device has been shown to be capable of high-throughput separation of cells using machined electrodes with dimensions similar to those used in photolithographic systems. Using our present system a throughput of 25 μl/h^{-1} has been shown to be possible, but the nature of the device lends itself to high degrees of parallelization. A similar device, with bores covering a radius of 60 mm should theoretically be able to process 1 L/h^{-1}. Such a system may greatly extend the implementation of dielectrophoretic devices in a broad range of industrial applications.

References

[1] H. A. Pohl, *Dielectrophoresis*, Cambridge, U.K.: Cambridge Univ. Press, 1978.

[2] M. P. Hughes, *Nanoelectromechanics in Engineering and Biology*. Boca Raton, FL: CRC, 2002.

[3] F. H. Labeed, H. M. Coley, H. Thomas, and M. P. Hughes, "Assessment of multidrug resistance reversal using dielectrophoresis and flow cytometry," *Biophys. J.*, vol. 85, pp. 2028–2034, 2003.

[4] J. Johari, Y. Hübner, J. C. Hull, J. W. Dale, and M. P. Hughes, "Dielectrophoretic assay of bacterial resistance to antibiotics," *Phys. Med. Biol.*, vol. 48, pp. N193–N196, 2003.

[5] Y. Hübner, K. F. Hoettges, and M. P. Hughes, "Water quality test based on dielectrophoretic measurements of fresh water algae Selenastrum capricornutum," *J. Env. Monitor*, vol. 5, pp. 861–864, 2003.

[6] M. P. Hughes, "Strategies for dielectrophoretic separation in laboratory-on-a-chip systems," *Electrophoresis*, vol. 23, pp. 2569–2582, 2002.

[7] S. S. Lee, F. M. Robinson, and H. Y. Wang, "Rapid determination of yeast viability," *Biotechnol. Bioeng.*, vol. 11, pp. 641–649, 1981.